Phys. Lett. B 869 (2025) 139856

Contents lists available at ScienceDirect

Physics Letters B

journal homepage: www.elsevier.com/locate/physletb

Letter

Joint analysis of reactor and accelerator CEνNS data on germanium: implications for the standard model and nuclear physics

M. Atzori Corona [a], M. Cadeddu [b], N. Cargioli [b], G. Co' [c], F. Dordei [b], C. Giunti [d]

[a] Istituto Nazionale di Fisica Nucleare (INFN), Sezione di Roma Tor Vergata, Via della Ricerca Scientifica, I-00133, Rome, Italy
[b] Istituto Nazionale di Fisica Nucleare (INFN), Sezione di Cagliari, Complesso Universitario di Monserrato - S.P. per Sestu Km 0.700, 09042, Monserrato, Cagliari, Italy
[c] Dipartimento di Matematica e Fisica E. De Giorgi" Università del Salento, Istituto Nazionale di Fisica Nucleare (INFN), Sezione di Lecce via Arnesano, Lecce, 73100, Italy
[d] Istituto Nazionale di Fisica Nucleare (INFN), Sezione di Torino, Via P. Giuria 1, I-10125, Torino, Italy

ARTICLE INFO

Editor: Baha Balantekin

Keywords:
Coherent elastic neutrino nucleus scattering
Neutron radius
Electroweak interaction
Weak mixing angle
Neutrino charge radius

ABSTRACT

This work presents the first comprehensive joint analysis of all available Coherent Elastic Neutrino-Nucleus Scattering (CEνNS) data on germanium: those observed at the Spallation Neutron Source (SNS) by the COHERENT collaboration and those of the nuclear reactors revealed by the CONUS+ experiment using germanium detectors. In addition to COHERENT and CONUS+, we incorporate reactor data from TEXONO and νGeN, thereby enhancing both the statistical significance and the systematic reliability of our study. We provide state-of-the-art determinations of key nuclear physics and Standard Model parameters, including the neutron root-mean-square (rms) radius of germanium nuclei, the weak mixing angle, and the neutrino charge radius. The observed tension of about 2σ between the COHERENT germanium measurement and the Standard Model prediction motivates a detailed reassessment of the theoretical cross-section. In particular, we examine the impact of nuclear form factors and uncertainties in the nuclear radius, as well as the potential influence of a systematic shift in the neutrino flux normalisation at the SNS. Our results highlight the reliability of CEνNS as a precision tool, reinforced by the complementarity of different experimental inputs, and lay the groundwork for future advances in the field.

1. Introduction

Coherent elastic neutrino-nucleus scattering (CEνNS), first predicted in 1974 [1], has emerged in recent years as a powerful low-energy probe for both testing the Standard Model (SM) and searching for phenomena beyond it [2,3]. This process was first observed in 2017 by the COHERENT collaboration [4–6] using a CsI detector exposed to the stopped-pion neutrino source at the Spallation Neutron Source (SNS), and subsequently confirmed using a liquid argon target [7]. These landmark results opened the door to precision neutrino physics in the low-energy regime [8–30,30,31,31–42], stimulating a new generation of CEνNS experiments across various platforms.

A major step forward has now been achieved with the first observation of CEνNS on a germanium target with an active mass of (10.66 ± 0.09) kg at the SNS, as reported by the COHERENT collaboration [43]. This marks the first CEνNS detection from a pion-decay-at-rest neutrino source on a high-purity germanium detector, adding a crucial third nuclear target to the experimental landscape. This result has been implemented with the recent CEνNS observations by the CONUS+ [44] collaboration using reactor antineutrinos on a similar germanium target, representing the first unambiguous CEνNS detection at a reactor site.

These two independent observations on germanium, realised under very different neutrino flux conditions, namely prompt, pulsed neutrinos from pion decay at the SNS versus steady, lower-energy antineutrinos from a commercial reactor, provide a unique opportunity for a simultaneous analysis. In reactor-based CEνNS experiments, such as those conducted by CONUS+ but also the recent intriguing constraints posed by the TEXONO [45] and νGeN [46] collaborations, the antineutrino energies are limited to a few MeV. At these low energies, the momentum transfer is small enough that the nuclear form factor remains essentially flat and close to unity. As a result, the scattering cross section becomes largely insensitive to nuclear structure effects, offering a cleaner experimental environment for probing fundamental SM parameters, neutrino properties and possible non-standard interactions.

On the other hand, CEνNS measurements at the SNS involve neutrinos in the tens-of-MeV range, where the finite momentum transfer begins to probe the nuclear interior, introducing sensitivity to nuclear models and related uncertainties. Moreover, while reactor data is only

E-mail addresses: mcorona@roma2.infn.it (M. Atzori Corona), matteo.cadeddu@ca.infn.it (M. Cadeddu), nicola.cargioli@ca.infn.it (N. Cargioli), giampaolo.co@le.infn.it (G. Co'), francesca.dordei@cern.ch (F. Dordei), carlo.giunti@to.infn.it (C. Giunti).

https://doi.org/10.1016/j.physletb.2025.139856
Received 18 June 2025; Accepted 27 August 2025
Available online 1 September 2025

sensitive to the electronic flavour, accelerator data offers a unique opportunity to probe both electron and muon neutrino flavours.

This complementarity between reactor and accelerator sources is especially valuable when considering data from a common target such as germanium. We present the first combined analysis of CEνNS results on germanium, integrating data from both SNS and reactor-based experiments. We provide state-of-the-art determinations of key nuclear physics parameters such as the neutron root-mean-square (rms) radius of germanium nuclei and fundamental SM quantities, including the weak mixing angle, and the neutrino charge radius.

2. Theory

The CEνNS differential cross section as a function of nuclear recoil energy T_{nr} for a neutrino ν_ℓ ($\ell = e, \mu, \tau$) scattering off a nucleus $\mathcal{N}$ with Z protons and N neutrons is [2][1]

$$\frac{d\sigma_{\nu_\ell\text{-}\mathcal{N}}}{dT_{\mathrm{nr}}} = \frac{G_{\mathrm{F}}^2 M}{\pi}\left(1 - \frac{M T_{\mathrm{nr}}}{2E^2}\right)\left(Q^V_{\ell,\mathrm{SM}}\right)^2, \tag{1}$$

where G_{F} is the Fermi constant, E the neutrino energy, M the nuclear mass[2] and the weak nuclear charge is

$$Q^V_{\ell,\mathrm{SM}} = \left[g_V^p(\nu_\ell) Z F_Z(|\vec{q}|^2) + g_V^n N F_N(|\vec{q}|^2)\right]. \tag{2}$$

We indicate with F_Z and F_N the proton and neutron form factors of the nucleus and with g_V^n and g_V^p the coefficients which quantify the weak neutral-current interactions of neutrons and protons. In the SM, the values of these coefficients are [25]

$$g_V^p(\nu_e) = 0.0379,\ g_V^p(\nu_\mu) = 0.0297, \tag{3}$$

$$g_V^p(\nu_\tau) = 0.0253,\ g_V^n = -0.5117, \tag{4}$$

when taking into account radiative corrections in the $\overline{\mathrm{MS}}$ scheme [24,48,49]. The flavor dependence of $g_V^p(\nu_\ell)$ is due to the neutrino charge radii (CR), which represent the only non-zero electromagnetic properties of neutrinos in the SM [50]. The SM neutrino CR prediction can be written as [51,52]

$$\langle r^2_{\nu_\ell}\rangle_{\mathrm{SM}} = -\frac{G_{\mathrm{F}}}{2\sqrt{2}\pi^2}\left[3 - 2\ln\left(\frac{m_\ell^2}{m_W^2}\right)\right], \tag{5}$$

where m_W is the W boson mass, m_ℓ is the mass of the charged lepton $\ell = e, \mu, \tau$. The SM values of the neutrino CR of interest for this work are:

$$\langle r^2_{\nu_e}\rangle_{\mathrm{SM}} \simeq -0.83 \times 10^{-32}\ \mathrm{cm}^2, \tag{6}$$

$$\langle r^2_{\nu_\mu}\rangle_{\mathrm{SM}} \simeq -0.48 \times 10^{-32}\ \mathrm{cm}^2. \tag{7}$$

The proton, $F_Z(|\vec{q}|^2)$, and neutron, $F_N(|\vec{q}|^2)$, nuclear form factors (FFs) in Eq. (2) encode the dependence of the process on the nuclear structure, and are defined as the Fourier transform of the corresponding nucleon density distributions in the nucleus, $\rho_{Z(N)}$, respectively. Their effect becomes more relevant for increasing momentum transfers, $|\vec{q}| \simeq \sqrt{2MT_{\mathrm{nr}}}$ [15] leading to a suppression of the full coherence [24] in the CEνNS process. As stated in the introduction, while the FFs are crucial ingredients in the interpretation of COHERENT data, in the low-energy regime of reactor experiments, the FF of both protons and neutrons is practically equal to unity, making the particular choice of the parameterisation almost irrelevant. We employ the analytical Helm parameterisation to describe both proton and neutron FFs [53]. This parameterisation is practically equivalent to other two well-known parameterisations, i.e., the symmetrised Fermi [54] and Klein-Nystrand [55] ones.

[1] In this work we use natural units such that $\hbar = c = 1$.

[2] For the isotopic composition of germanium, we use the values from Ref. [47].

Table 1
Proton (R_p) and neutron (R_n) root-mean-square radii for germanium isotopes. The experimental values of R_p are derived from the measured charge radii reported in Ref. [56], using the procedure described in Ref. [18]. The theoretical values are those obtained from HF + BCS calculations carried out with the D1S [59] and D1M [60] interactions, and from NSM predictions [61].

	R_p [fm]			R_n [fm]		
	Ref. [56]	D1S [59]	D1M [60]	D1S [59]	D1M [60]	NSM [61]
^{70}Ge	4.055(1)	3.99	3.93	4.02	3.97	4.14
^{72}Ge	4.073(1)	4.01	3.96	4.07	4.02	4.20
^{73}Ge	4.079(1)	4.03	3.97	4.10	4.04	4.22
^{74}Ge	4.091(1)	4.05	3.98	4.13	4.06	4.26
^{76}Ge	4.099(1)	4.06	3.99	4.16	4.10	4.30

The Helm form factor depends on the rms radius of protons and neutrons. While the proton rms radii can be obtained from the charge radius [18], which is extracted from muonic atom spectroscopy and electron scattering data [56–58], the neutron rms radii lack precise measurements for the target nuclei employed in CEνNS experiments. Therefore, some assumptions need to be made.

Here, we consider the values obtained from the recent nuclear shell model (NSM) estimate of the corresponding neutron skins (i.e. the differences between the neutron and the proton rms radii) in Ref. [61] (see also Ref. [62]). The considered proton and neutron rms radii are summarized in Table 1.

Given that the differences in the prediction for the radii of different isotopes is below the current experimental precision, when using the Helm phenomenological model, we consider as a reference for our analysis the average values of the nuclear rms proton and neutron radii weighted by the isotopic composition, namely 4.08 fm and 4.22 fm respectively. Moreover, we investigate the uncertainties related to the nuclear model [63] by considering also proton and neutron density distributions obtained by carrying out Hartree-Fock plus Bardeen-Cooper-Schrieffer calculations (HF + BCS) [64]. These calculations have been performed by using two different parameterisations of the effective nucleon-nucleon finite-range interaction of Gogny type, namely the D1M [60] and the D1S [59] forces. The corresponding rms proton and neutron distribution radii have been reported in Table 1. Therefore, the FF for protons (neutrons) is evaluated as

$$\begin{aligned} F_{Z(N)} &= \frac{1}{Z(N)}\int d^3r\, e^{i\mathbf{q}\cdot\mathbf{r}}\rho_{Z(N)}(r) \\ &= \frac{4\pi}{Z(N)}\int_0^\infty dr\, r^2\, \rho_{Z(N)}(r) j_0(qr), \end{aligned} \tag{8}$$

where j_0 is the zero-order Bessel function.

We show in Fig. 1 (a) the neutron densities of the ^{76}Ge nucleus obtained by the HF + BCS calculation and compare it with our reference Helm neutron distribution obtained by considering the average neutron rms radius $R_n^{\mathrm{NSM}} = 4.22$ fm. In Fig. 1 (b) we show the related FFs. The sensitivity of the CEνNS results to the use of the different FFs is discussed in the next section.

3. Anaysis of CEνNS data

We analysed the reactor CONUS + [44] and TEXONO [45] data by using the procedure outlined in detail in Ref. [65]. We consider, in addition, the data of the recent νGeN CEνNS experiment [46], which employs a 1.41 kg high-purity, low-threshold germanium detector located at 11.1 m from the Kalinin Nuclear Power Plant. We parametrize the νGeN reactor neutrino flux using the prescriptions of Ref. [66], which yields a total neutrino flux of $\Phi_{\mathrm{est}} \simeq 4.4 \times 10^{13}\ \nu/(\mathrm{s\ cm}^2)$. Hereafter, we will refer to the joint analysis of CONUS + , νGeN and TEXONO data as `Reactors`.

When needed for comparisons, the COHERENT CsI [67] and Ar [7,68] data are analysed following the strategy explained in detail in

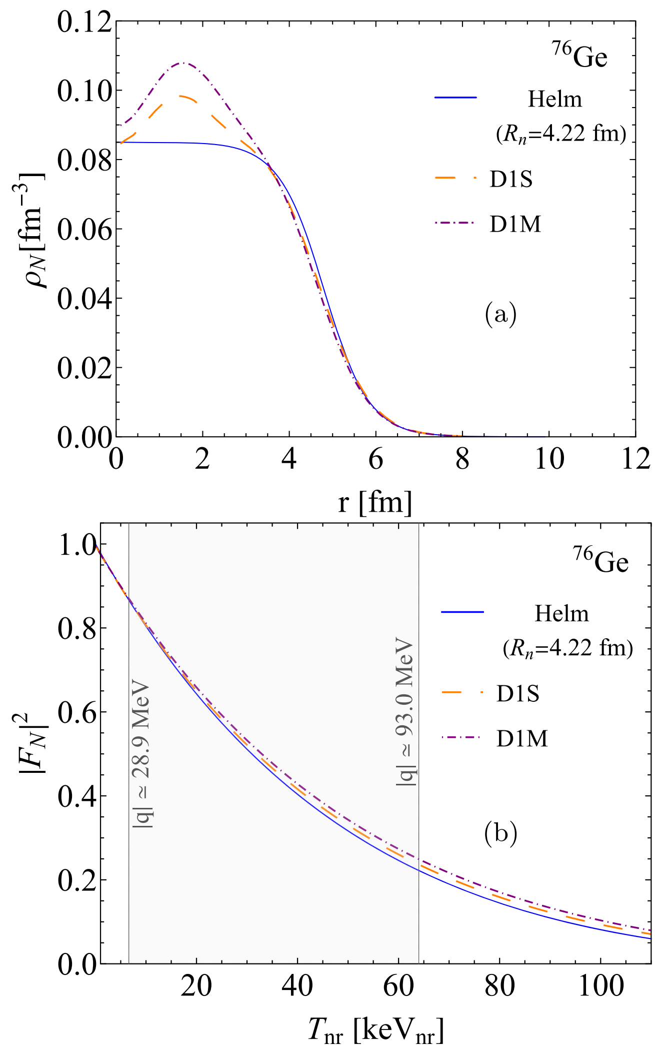

Fig. 1. (a) Neutron density distributions of the ^{76}Ge nucleus obtained with the Helm model by using an average neutron rms radius $R_n^{\rm NSM} = 4.22$ fm as indicated by the NSM [61] (solid blue line) and with HF + BCS calculations obtained by using the D1M (dashed-dotted purple) or D1S (dashed orange) Gogny forces. (b) Related FFs, see Eq. (8), of the neutron densities shown in panel (a). The gray area indicates the region of interest of the COHERENT germanium experiment. (For interpretation of the references to colour in this figure legend, the reader is referred to the web version of this article.)

Refs. [22,24]. For the COHERENT Ge analysis, we instead follow the procedure described in Ref. [43] and the prescriptions summarised in the following. The total neutrino flux from pion decays at rest includes three components: prompt ν_μ's from pion decay, and the ν_e and $\bar{\nu}_\mu$ delayed components, from the subsequent muon decay. The neutrino flux depends on the number of protons-on-target $N_{\rm POT} = 1.96 \times 10^{22}$, the number of neutrinos produced for each POT, (0.288 ± 0.029), and the baseline between the source and the detector, $L = 19.2$ m [68]. In each nuclear-recoil energy-bin i, the expected CEνNS event number $N_i^{\rm CE\nu NS}$ on a germanium target is given by

$$N_i^{\rm CE\nu NS} = N_T \int_{T_{\rm nr}^i}^{T_{\rm nr}^{i+1}} dT_{\rm nr}\, A(T_{\rm nr}) \int_0^{T_{\rm nr}'^{\rm max}} dT'_{\rm nr}\, R(T_{\rm nr}, T'_{\rm nr}) \times \int_{E_{\rm min}(T'_{\rm nr})}^{E_{\max}} dE \sum_{\nu_\ell = \nu_e, \nu_\mu, \bar{\nu}_\mu} \frac{dN_{\nu_\ell}}{dE} \frac{d\sigma_{\nu_\ell - \mathcal{N}}}{dT'_{\rm nr}}. \tag{9}$$

Here, dN_{ν_ℓ}/dE is the neutrino flux, $T_{\rm nr}$ is the reconstructed nuclear recoil kinetic energy, $T'_{\rm nr}$ is the true nuclear recoil kinetic energy, $A(T_{\rm nr})$ is the energy-dependent detector efficiency [43], $R(T_{\rm nr}, T'_{\rm nr})$ is the energy resolution [43], $T_{\rm nr}'^{\rm max} \simeq 2E_{\rm max}^2/M$, $E_{\rm max} = m_\mu/2 \sim 52.8$ MeV, $E_{\rm min}(T'_{\rm nr}) \simeq \sqrt{MT'_{\rm nr}/2}$, m_μ being the muon mass, and N_T is the number of target atoms in the detector per unit mass. It is important to consider that the energy actually observed in the detector is the electron-equivalent recoil energy T_e, which is transformed into the nuclear recoil energy $T_{\rm nr}$ in the CEνNS rate by inverting the relation

$$T_{\rm e} = f_Q(T_{\rm nr}) T_{\rm nr}. \tag{10}$$

Here f_Q is the quenching factor, whose dependence on the recoil energy is still being actively investigated. A precise understanding of its behaviour is essential for interpreting experimental results [69,70], with important consequences for the extraction of SM and beyond parameters [71]. In this work we adopt the Lindhard model [72] with $k = 0.162 \pm 0.004$ as measured by the CONUS Collaboration [73]. Accounting for the time structure of the COHERENT data is crucial for distinguishing between the different neutrino components. We extract the arrival-time distribution of the different neutrino components from Ref. [74], and incorporate the timing information by dividing the theoretical CEνNS event numbers $N_i^{\rm CE\nu NS}$ in Eq. (9) into time bins of 4 μs. This yields $N_{ij}^{\rm CE\nu NS}$, where i and j label the energy and time bins, respectively. To compare the prediction with the data, we perform a simultaneous fit of beam-on (ON) and beam-off (OFF) data by using the least-squares function [43]

$$\chi^2 = \chi^2_{\rm ON}(\eta, \beta) + \chi^2_{\rm OFF}(\beta) + \left(\frac{\eta - 1}{\sigma_\eta}\right)^2 + \left(\frac{\beta - 1}{\sigma_\beta}\right)^2, \tag{11}$$

where

$$\chi^2_{\rm ON} = 2 \sum_{\substack{i=1 \\ i \neq \{4,5\}}}^{9} \sum_{j=1}^{10} \left(\eta N_{ij}^{\rm CE\nu NS} + \beta N_{ij}^{\rm SSB} - N_{ij}^{\rm exp,\,ON} + N_{ij}^{\rm exp,\,ON} \ln\left[\frac{N_{ij}^{\rm exp,\,ON}}{\eta N_{ij}^{\rm CE\nu NS} + \beta N_{ij}^{\rm SSB}}\right]\right), \tag{12}$$

and

$$\chi^2_{\rm OFF} = 2 \sum_{\substack{i=1 \\ i \neq \{4,5\}}}^{9} \sum_{j=1}^{10} \left(\beta N_{ij}^{\rm SSB} - N_{ij}^{\rm exp,\,OFF} + N_{ij}^{\rm exp,\,OFF} \ln\left[\frac{N_{ij}^{\rm exp,\,OFF}}{\beta N_{ij}^{\rm SSB}}\right]\right). \tag{13}$$

Here, we are following the prescription from the COHERENT collaboration to remove the energy bins in the range [8.5, 11.5] keV$_{\rm ee}$,[3] which corresponds to $i = 4, 5$ [43]. Moreover, $N_{i,j}^{\rm exp,ON\,(OFF)}$ is the observed number of events from beam-ON (OFF) data as extracted from Ref. [43] in the ith (energy) and jth (time) bin, while $N_{ij}^{\rm SSB}$ is the steady state background (SSB) from internally-triggered data. The latter is extracted from Fig. 3 of Ref. [43], where the spectral shape of the SSB is provided in a 40 µs time window, for the exposure of the beam-ON data set. The two-dimensional distribution of the SSB is obtained by assuming it to be constant over time. Finally, $N_{i,j}^{\rm CE\nu NS}$ is the predicted number of CEνNS events that depends on the physics model under consideration. The systematic uncertainty on the signal prediction is $\sigma_\eta = 10.3\,\%$ and it is dominated by the uncertainty on the neutrino flux (10 %), but includes also the uncertainty on the detector location (0.5 %), energy calibration (1 %), active mass (1 %) and form factors (1 %). The systematic uncertainty on the SSB is $\sigma_\beta = 1\,\%$, thanks to the fact that the simultaneous fit of ON and OFF data allows one to constrain the normalisation of the SSB in the fit precisely.

[3] It is important to highlight that due the 2D binning of the data provided by the COHERENT collaboration, we are excluding the energy range [7.5, 11.5] keV$_{\rm ee}$, while the official result excludes the energy range [8.5, 11.5] keV$_{\rm ee}$.

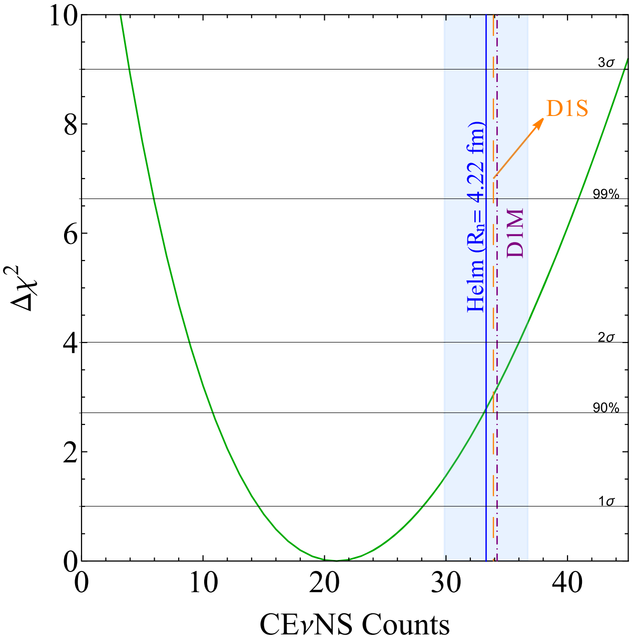

Fig. 2. Marginal $\Delta\chi^2$ profile as a function of the number of CEνNS events. For comparison, the CEνNS prediction for different nuclear models is shown by the vertical lines: using a Helm neutron FF with an average neutron rms radius $R_n^{\mathrm{NSM}} = 4.22$ fm as predicted by NSM [61] (solid blue), or parameterizing the nuclear density distribution with a D1M (dashed-dotted purple) or D1S (dashed orange) Gogny type model. The light blue area indicates the systematic uncertainty on the theoretical prediction $\sigma_\eta = 10.3\,\%$. (For interpretation of the references to colour in this figure legend, the reader is referred to the web version of this article.)

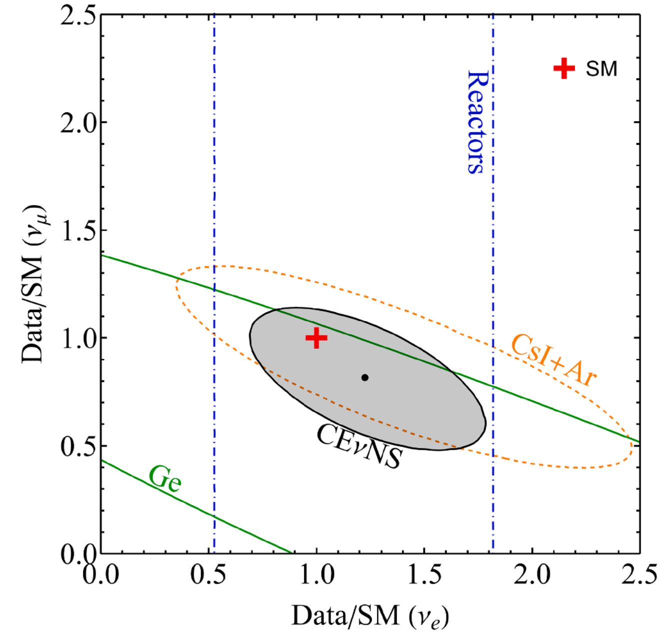

Fig. 3. Agreement between CEνNS data and SM predictions for COHERENT CsI + Ar (orange dashed contour), reactors (blue dotted-dashed band), COHERENT germanium (green solid contour) and the combined analysis (black region), separate for electron and muon neutrinos. Contours are shown at 90 % CL, and the black point represents the best-fit, while the red cross indicates perfect agreement with the SM prediction. (For interpretation of the references to colour in this figure legend, the reader is referred to the web version of this article.)

We employ Eq. (11) to extract the experimental number of CEνNS events obtained leaving the CEνNS normalisation free to vary in the fit, while removing the systematic uncertainty σ_η. The marginal $\Delta\chi^2 = \chi^2 - \chi^2_{\mathrm{min}}$ distribution is shown in Fig. 2, which is in excellent agreement with that released by the COHERENT collaboration [43]. We find about $21.0^{+7.1}_{-6.4}$ CEνNS events, which should be compared with our theoretical prediction of 33.3 ± 3.4 events assuming a Helm neutron FF with an average neutron rms radius $R_n^{\mathrm{NSM}} = 4.22$ fm from NSM, which increases to 33.9 ± 3.5 (34.2 ± 3.5) considering the D1S (D1M) model for the neutron nuclear density. Our theoretical prediction obtained using the NSM is 1.7σ above the best-fit value. This small tension increases to about 1.8σ when assuming the D1S and D1M nuclear models.

In order to search for potential flavour-dependent effects in the COHERENT germanium data and exploit the power of the timing information, we split the signal normalisation, $\eta = \mathrm{Data/SM}$, according to the neutrino flavour. This strategy, introduced in Ref. [65], allows for a meaningful comparison with reactor CEνNS data, which are sensitive only to the ν_e flavour. The result is shown in Fig. 3 at the 90 % confidence level (CL). Within this combined analysis, we find a general agreement among all CEνNS probes, obtaining

$$\begin{aligned}\mathrm{Data/SM}\,(\nu_e) &= 1.24^{+0.25}_{-0.26}(1\sigma),^{+0.42}_{-0.43}\,(90\,\%),^{+0.51}_{-0.52}\,(2\sigma),\\ \mathrm{Data/SM}\,(\nu_\mu) &= 0.78^{+0.17}_{-0.14}(1\sigma),^{+0.27}_{-0.24}\,(90\,\%),^{+0.33}_{-0.29}\,(2\sigma).\end{aligned} \quad (14)$$

The best fit indicates a preference for a slightly higher normalisation of the electronic flavour, but consistent with the SM within 1σ, while a slight under fluctuation is observed for the muonic flavour, at the 1σ level. Nevertheless, both normalisations remain consistent with one at the 90 % CL. Future datasets with improved statistical precision will allow for a more accurate testing of SM predictions.

4. Implications for electroweak and nuclear physics

In Fig. 4 we show the constraints on the value of the weak mixing angle, $\sin^2\vartheta_W$, from the COHERENT Ge data-set, by fixing the neutron nuclear radius to the theoretical predictions from NSM and the D1S model (which practically overlaps with the D1M one). We notice that the extracted values of the weak mixing angle are not strongly dependent on the parameterisation of the nuclear structure, making CEνNS a robust probe for studying SM key parameters. In the same figure, we also show the constraints from the joint CsI [24] and Ar [18] analysis, from reactor data, i.e. CONUS +, TEXONO with the inclusion of νGeN, and the result of a combined analysis when fixing the neutron nuclear radius to the NSM prediction. The result of this combined analysis is

$$\sin^2\theta_W = 0.229^{+0.020}_{-0.019}\,(1\sigma),^{+0.040}_{-0.037}\,(2\sigma), \pm 0.06\,(3\sigma). \quad (15)$$

This result represents the state-of-the-art determination on the low-energy value of the weak mixing angle from CEνNS probes, and it is consistent with the SM and the recent re-evaluation in Ref. [75].

When using electroweak probes with nuclei, the weak mixing angle is known to be correlated with the neutron nuclear radius [19,21,24,75,76]. Therefore, we also perform a two-dimensional analysis by considering both $\sin^2\vartheta_W$ and $R_n(\mathrm{Ge})$ as free parameters. The outcome is shown in Fig. 5, where we also display the result of a fit to reactor germanium data under this configuration. This result clearly highlights the complementarity between the findings obtained by fitting data from accelerator-based neutrino experiments and those from reactor-based experiments. The former exhibits a band with a strong correlation between the weak mixing angle and the neutron nuclear radius. On the contrary the reactor CEνNS data are practically insensitive to $R_n(\mathrm{Ge})$. To further restrict the phase-space available on the weak mixing angle, in our analysis we also consider low-energy $\nu - e^-$ scattering data from TEXONO [77], LSND [78], LAMPF [79], LZ [80], PandaX [81] and XENONnT [82] electron recoil data, as described in Ref. [3]. By using

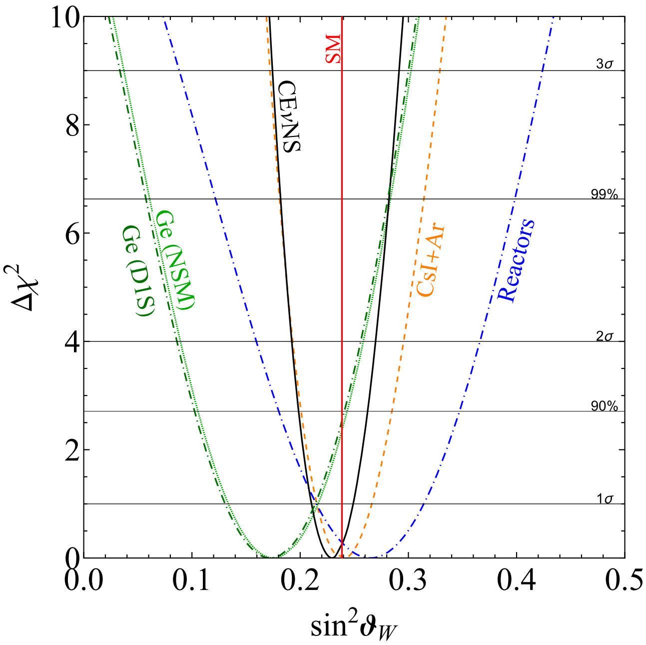

Fig. 4. Constraints on the weak mixing angle at different confidence levels from the joint analysis of CsI and Ar data (dashed orange), reactors (dashed-dotted blu) and COHERENT germanium (green), the latter assuming two different parameterisations for the nuclear structure. The combined analysis is shown in black while the SM prediction is shown by the red vertical line. (For interpretation of the references to colour in this figure legend, the reader is referred to the web version of this article.)

all these data we obtain a clean low-energy determination of the weak mixing angle, which is independent of the neutron nuclear radius.

By combining all these inputs we find, at the 1σ CL, the following values

$$\sin^2\vartheta_W = 0.271^{+0.023}_{-0.026}; \quad R_n(\mathrm{Ge}) = 7.6^{+1.6}_{-1.7}\ \mathrm{fm}. \tag{16}$$

The value of the nuclear neutron radius emerging from this analysis is exceptionally high with respect to those obtained in the HF+BCS calculations and excludes the NSM prediction [61] at about 2σ. This disagreement is driven by the positive correlation of $R_n(\mathrm{Ge})$ and $\sin^2\vartheta_W$ in COHERENT data. In addition, we remark that the $\nu - e^-$ scattering data slightly prefer higher $\sin^2\vartheta_W$ values than those indicated by the SM, and this selects a region of the parameter space in disagreement with expectations. The adoption of the best-fit values in Eq. (16) improves the fit to COHERENT Ge data by $\Delta\chi^2 \simeq -2.7$, when compared to the use of the expected SM and NSM $\sin^2\vartheta_W$ and $R_n(\mathrm{Ge})$ values, respectively. This can be physically explained by the fact that a larger nuclear radius is responsible for an enhanced suppression in the cross section, which makes the prediction more in agreement with the under-fluctuations of events observed in the COHERENT Ge data.

We also evaluated the constraints on the average rms germanium nuclear radius when fixing the weak mixing angle to its SM value, namely 0.23873 ± 0.00005 [49], and we obtain

$$R_n(\mathrm{Ge}) = 6.5 \pm 1.4\,(1\sigma), \pm 3.0\,(2\sigma), < 11.8\,(3\sigma)\ \mathrm{fm}. \tag{17}$$

It is worth highlighting that the fact that the COHERENT collaboration removed the energy bins in the range $[7.5, 11.5]\ \mathrm{keV_{ee}}$, which corresponds to $[27.5, 39.0]\ \mathrm{keV_{nr}}$, is not beneficial for accurate studies of the nuclear structure, as a crucial part of the spectral shape information is lost. In fact, in this energy regime, the nuclear neutron form factor $|F_N|^2$

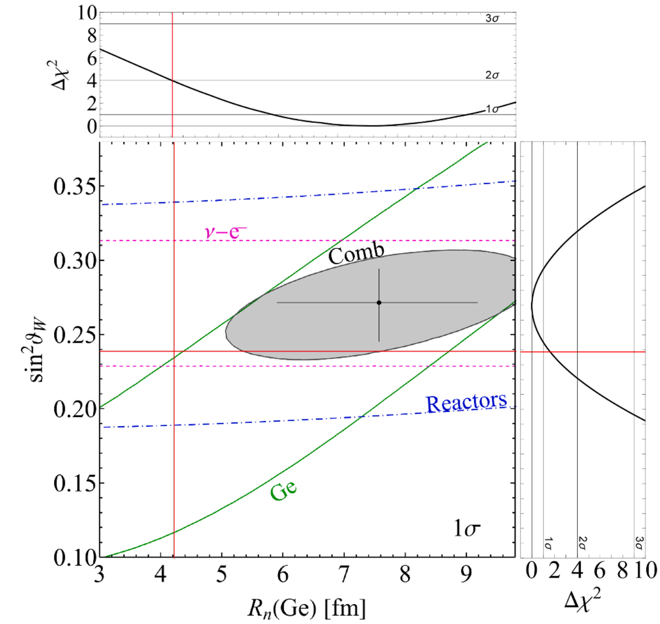

Fig. 5. Constraints obtained by fitting the weak mixing angle and the average rms Ge neutron radius on COHERENT Ge data (solid green band) and reactors (dashed-dotted blue band), as well as the prior on the weak mixing angle from $\nu - e^-$ data (dashed magenta band) and the result of a combined analyis (black contour) at 1σ CL. The upper (right) panel shows the one-dimensional marginalisation on neutron radius (weak mixing angle) from the combined analysis at different CLs. The red lines indicate the SM low-energy value of the weak mixing angle and the NSM prediction for $R_n(\mathrm{Ge})$. (For interpretation of the references to colour in this figure legend, the reader is referred to the web version of this article.)

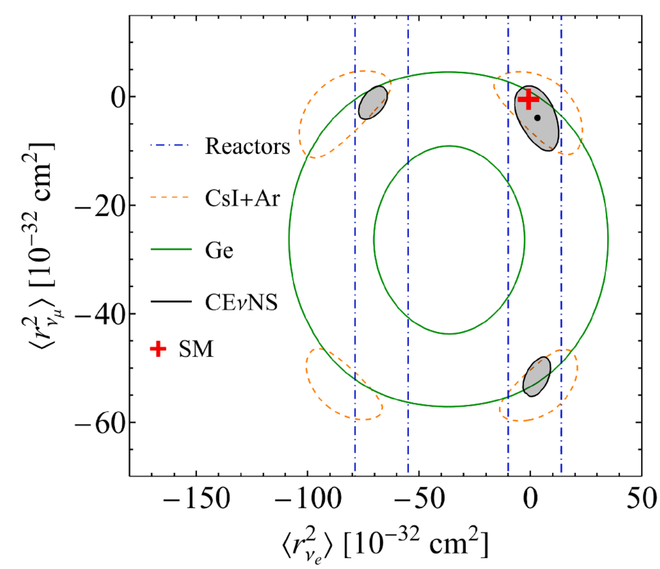

Fig. 6. Allowed regions at 90% CL on the electronic and muonic neutrino charge radii considering a momentum-dependence in the neutrino charge radii radiative corrections [25], from the analysis COHERENT germanium, COHERENT CsI and Ar, reactor CEνNS data, together with their combined analysis. The red cross indicates the SM values reported in Eqs. (6) and (7), while the black dot represents the best-fit of the combined analysis. (For interpretation of the references to colour in this figure legend, the reader is referred to the web version of this article.)

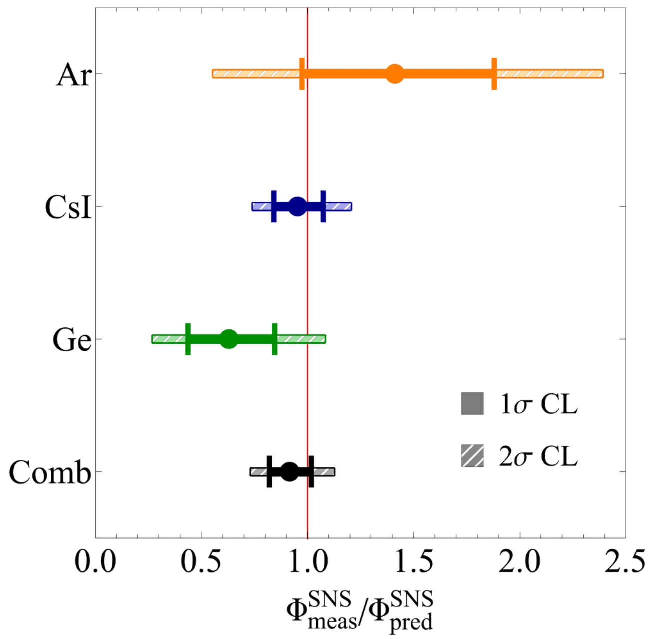

Fig. 7. Measured neutrino flux at the SNS relative to the total expected neutrino flux during the full data-taking period for Ar, CsI, and Ge data and their combination.

varies from $[0.56, 0.44]$ when assuming the nuclear radius from nuclear shell models, as shown in Fig. 1del (b). Moreover, a CEνNS analysis in the full energy spectrum would not only be relevant to reduce the uncertainty on R_n(Ge), but would also be crucial to search for insights beyond the nuclear theory.

Another fundamental SM parameter which can be constrained by CEνNS processes is the neutrino charge radius. Here, we also account for the momentum-dependence of the neutrino charge-radius radiative correction, as described in Ref. [25]. The results of the fit to all available CEνNS data are summarised in Fig. 6 by using a $\langle r^2_{\nu_e}\rangle$ and $\langle r^2_{\nu_\mu}\rangle$ plane. Due to the limited statistics, at 90 % CL COHERENT Ge displays a full degeneracy among these two parameters which can be broken thanks to the complementarity with reactor data which are only sensitive to the electronic neutrino flavour. Intriguingly, even if the 2D contours in Fig. 6 present three degenerate regions at the 90 % CL, when considering 2 degrees of freedom ($\Delta\chi^2 = 4.6$), the corresponding marginal 1D distributions select the SM region at the 1σ CL for both flavors, namely

$$\langle r^2_{\nu_e}\rangle = (3.2 \pm 4.7) \times 10^{-32}\,\mathrm{cm}^2, \tag{18}$$

$$\langle r^2_{\nu_\mu}\rangle = -\,3.9^{+2.8}_{-2.7} \times 10^{-32}\,\mathrm{cm}^2. \tag{19}$$

5. Interpretations and conclusions

We investigate the possible sources of the small discrepancy between theoretical predictions and data of the COHERENT germanium dataset. Nuclear physics does not appear to resolve this issue, as the best-fit value for the neutron rms radius is found to be unphysically large, see Eq. (16). Invoking physics Beyond the Standard Model (BSM) is also challenging in this case, as most BSM scenarios, such as neutrino magnetic moments, millicharges, or light mediator bosons, typically predict an excess of events compared to the SM, whereas the germanium data shows a deficit.

We therefore focus on a possible systematic effect related to the neutrino flux measured at the SNS, $\Phi^{\rm SNS}_{\rm meas}$, which represents the dominant uncertainty in the CEνNS signal. To explore this, we show in Fig. 7 the constraints obtained by allowing the normalisation of the SNS neutrino flux to vary freely in the fit. This normalisation is taken relative to the total predicted neutrino flux, $\Phi^{\rm SNS}_{\rm pred}$, during the data-taking period. We obtain

$$\text{Ar:}\quad \frac{\Phi^{\rm SNS}_{\rm meas}}{\Phi^{\rm SNS}_{\rm pred}} = 1.4^{+0.5}_{-0.4}\,(1\sigma),^{+1.0}_{-0.9}\,(2\sigma), \tag{20}$$

$$\text{CsI:}\quad \frac{\Phi^{\rm SNS}_{\rm meas}}{\Phi^{\rm SNS}_{\rm pred}} = 0.95^{+0.12}_{-0.11}\,(1\sigma),^{+0.25}_{-0.21}\,(2\sigma), \tag{21}$$

$$\text{Ge:}\quad \frac{\Phi^{\rm SNS}_{\rm meas}}{\Phi^{\rm SNS}_{\rm pred}} = 0.63^{+0.22}_{-0.19}\,(1\sigma),^{+0.46}_{-0.36}\,(2\sigma), \tag{22}$$

$$\text{Comb:}\quad \frac{\Phi^{\rm SNS}_{\rm meas}}{\Phi^{\rm SNS}_{\rm pred}} = 0.92 \pm 0.10\,(1\sigma),^{+0.21}_{-0.19}\,(2\sigma). \tag{23}$$

The combined result in Eq. (23) indicates a possible flux deficit, with a best-fit combined normalisation factor of 0.92. However, this value remains compatible with unity at the 1σ level and falls within the 10 % systematic uncertainty quoted by the collaboration. This downward fluctuation is primarily driven by the CsI and Ge datasets, while the Ar dataset shows a slight upward fluctuation, albeit with a much larger uncertainty.

Although this analysis does not provide conclusive evidence for a flux-related systematic effect that could explain the event deficit observed in COHERENT Ge, it clearly highlights the importance of reducing the associated uncertainty. For this purpose, COHERENT is developing a new detector [83] based on heavy water D_2O, which aims to reduce the neutrino flux uncertainty to the 2–3 % level. The detector will be positioned approximately 20 m from the SNS target and is expected to achieve better than 5 % statistical uncertainty on the neutrino flux within two years of operation. This heavy-water detector will also serve as the first module of a two-module system, ultimately designed to provide high-precision flux measurements. This will significantly improve the precision on both SM and BSM observables and help clarify whether the tension in the COHERENT Ge dataset is merely a statistical fluctuation or an indication of new physics.

Despite the small underfluctuation observed in the COHERENT germanium data, our combined analysis of all available CEνNS measurements yields a consistent and robust global picture. This joint fit enables precise determinations of the weak mixing angle and the neutrino charge radii, demonstrating the value of integrating diverse experimental inputs. In particular, the complementarity between accelerator- and reactor-based CEνNS experiments is essential to break parameter degeneracies and to reduce uncertainties. This unified approach not only maximises the scientific return of current data but also lays solid foundations for future precision CEνNS studies. As the field advances toward next-generation detectors with improved sensitivity, varied target materials, and broader physics goals, such global strategies will be essential to fully exploit the potential of CEνNS .

Data availability

We performed a phenomenology study using public data.

Declaration of competing interest

The authors declare that they have no known competing financial interests or personal relationships that could have appeared to influence the work reported in this paper.

Acknowledgments

The work of C. Giunti is partially supported by the PRIN 2022 research grant Number 2022F2843L funded by MIUR.

References

[1] D.Z. Freedman, Coherent neutrino nucleus scattering as a probe of the weak neutral current, Phys. Rev. D 9 (1974) 1389–1392. https://doi.org/10.1103/PhysRevD.9.1389

[2] M. Cadeddu, F. Dordei, C. Giunti, A view of coherent elastic neutrino-nucleus scattering, EPL 143 (3) (2023) 34001. arXiv:2307.08842 https://doi.org/10.1209/0295-5075/ace7f0

[3] M. Atzori Corona, M. Cadeddu, N. Cargioli, F. Dordei, C. Giunti, C.A. Ternes, The Standard Model tested with neutrinos, 2025. arXiv:2504.05272

[4] D. Akimov, et al., COHERENT, Observation of coherent elastic neutrino-nucleus scattering, Science 357 (6356) (2017) 1123–1126. arXiv:1708.01294 https://doi.org/10.1126/science.aao0990

[5] D. Akimov, et al., COHERENT Collaboration data release from the first observation of coherent elastic neutrino-nucleus scattering, 2018, arXiv:1804.09459 https://doi.org/10.5281/zenodo.1228631

[6] D. Akimov, et al., COHERENT, Measurement of the coherent elastic neutrino-nucleus scattering cross section on csi by COHERENT, Phys. Rev. Lett. 129 (8) (2022) 081801. arXiv:2110.07730 https://doi.org/10.1103/PhysRevLett.129.081801

[7] D. Akimov, et al., COHERENT, First measurement of coherent elastic neutrino-nucleus scattering on argon, Phys. Rev. Lett. 126 (1) (2021) 012002. arXiv:2003.10630 https://doi.org/10.1103/PhysRevLett.126.012002

[8] V. De Romeri, D.K. Papoulias, G. Sanchez Garcia, C.A. Ternes, M. Tórtola, Neutrino electromagnetic properties and sterile dipole portal in light of the first solar CEνNS data, 2024. arXiv:2412.14991

[9] D.Y. Akimov, et al., First constraints on the coherent elastic scattering of reactor antineutrinos off xenon nuclei, 2024. arXiv:2411.18641

[10] V. De Romeri, D.K. Papoulias, C.A. Ternes, Bounds on new neutrino interactions from the first CEνNS data at direct detection experiments, 2024, arXiv:2411.11749

[11] A. Majumdar, D.K. Papoulias, H. Prajapati, R. Srivastava, Constraining low scale Dark Hypercharge symmetry at spallation, reactor and Dark Matter direct detection experiments, 2024, arXiv:2411.04197

[12] V. Pandey, Recent progress in low energy neutrino scattering physics and its implications for the standard and beyond the standard model physics, Prog. Part. Nucl. Phys. 134 (2024) 104078. arXiv:2309.07840 https://doi.org/10.1016/j.ppnp.2023.104078

[13] P. Coloma, M.C. Gonzalez-Garcia, M. Maltoni, J.a.P. Pinheiro, S. Urrea, Global constraints on non-standard neutrino interactions with quarks and electrons, JHEP 08 (2023) 032. arXiv:2305.07698 https://doi.org/10.1007/JHEP08(2023)032

[14] D. Aristizabal Sierra, N. Mishra, L. Strigari, Implications of first neutrino-induced nuclear recoil measurements in direct detection experiments, 2024. arXiv:2409.02003

[15] M. Cadeddu, C. Giunti, Y.F. Li, Y.Y. Zhang, Average CsI neutron density distribution from COHERENT data, Phys. Rev. Lett. 120 (7) (2018) 072501. arXiv:1710.02730 https://doi.org/10.1103/PhysRevLett.120.072501

[16] M. Cadeddu, C. Giunti, K.A. Kouzakov, Y.-F. Li, Y.-Y. Zhang, A.I. Studenikin, Neutrino charge radii from coherent elastic neutrino-nucleus scattering, Phys. Rev. D 98 (11) (2018) 113010. arXiv:1810.05606 https://doi.org/10.1142/9789811233913_0013[Erratum: Phys.Rev.D 101, 059902 (2020)].

[17] M. Cadeddu, F. Dordei, C. Giunti, Y.F. Li, Y.Y. Zhang, Neutrino, electroweak, and nuclear physics from COHERENT elastic neutrino-nucleus scattering with refined quenching factor, Phys. Rev. D 101 (3) (2020) 033004. arXiv:1908.06045 https://doi.org/10.1103/PhysRevD.101.033004

[18] M. Cadeddu, F. Dordei, C. Giunti, Y.F. Li, E. Picciau, Y.Y. Zhang, Physics results from the first COHERENT observation of coherent elastic neutrino-nucleus scattering in argon and their combination with cesium-iodide data, Phys. Rev. D 102 (1) (2020) 015030. arXiv:2005.01645 https://doi.org/10.1103/PhysRevD.102.015030

[19] M. Cadeddu, F. Dordei, Reinterpreting the weak mixing angle from atomic parity violation in view of the Cs neutron rms radius measurement from COHERENT, Phys. Rev. D 99 (3) (2019) 033010. arXiv:1808.10202 https://doi.org/10.1103/PhysRevD.99.033010

[20] M. Cadeddu, N. Cargioli, F. Dordei, C. Giunti, Y.F. Li, E. Picciau, Y.Y. Zhang, Constraints on light vector mediators through coherent elastic neutrino nucleus scattering data from COHERENT, JHEP 01 (2021) 116. arXiv:2008.05022 https://doi.org/10.1007/JHEP01(2021)116

[21] M. Cadeddu, N. Cargioli, F. Dordei, C. Giunti, Y.F. Li, E. Picciau, C.A. Ternes, Y.Y. Zhang, New insights into nuclear physics and weak mixing angle using electroweak probes, Phys. Rev. C 104 (6) (2021) 065502. arXiv:2102.06153 https://doi.org/10.1103/PhysRevC.104.065502

[22] M. Atzori Corona, M. Cadeddu, N. Cargioli, F. Dordei, C. Giunti, Y.F. Li, E. Picciau, C.A. Ternes, Y.Y. Zhang, Probing light mediators and (g - 2) through detection of coherent elastic neutrino nucleus scattering at COHERENT, JHEP 05 (2022) 109. arXiv:2202.11002 https://doi.org/10.1007/JHEP05(2022)109

[23] M. Atzori Corona, M. Cadeddu, N. Cargioli, F. Dordei, C. Giunti, Y.F. Li, C.A. Ternes, Y.Y. Zhang, Impact of the Dresden-II and COHERENT neutrino scattering data on neutrino electromagnetic properties and electroweak physics, JHEP 09 (2022) 164. arXiv:2205.09484 https://doi.org/10.1007/JHEP09(2022)164

[24] M. Atzori Corona, M. Cadeddu, N. Cargioli, F. Dordei, C. Giunti, G. Masia, Nuclear neutron radius and weak mixing angle measurements from latest COHERENT CsI and atomic parity violation Cs data, Eur. Phys. J. C 83 (7) (2023) 683. arXiv:2303.09360 https://doi.org/10.1140/epjc/s10052-023-11849-5

[25] M. Atzori Corona, M. Cadeddu, N. Cargioli, F. Dordei, C. Giunti, Momentum dependent flavor radiative corrections to the coherent elastic neutrino-nucleus scattering for the neutrino charge-radius determination, JHEP 05 (2024) 271. arXiv:2402.16709 https://doi.org/10.1007/JHEP05(2024)271

[26] P. Coloma, M.C. Gonzalez-Garcia, M. Maltoni, T. Schwetz, COHERENT enlightenment of the neutrino dark side, Phys. Rev. D 96 (11) (2017) 115007. arXiv:1708.02899 https://doi.org/10.1103/PhysRevD.96.115007

[27] J. Liao, D. Marfatia, COHERENT constraints on nonstandard neutrino interactions, Phys. Lett. B 775 (2017) 54–57. arXiv:1708.04255 https://doi.org/10.1016/j.physletb.2017.10.046

[28] M. Lindner, W. Rodejohann, X.-J. Xu, Coherent neutrino-nucleus scattering and new neutrino interactions, JHEP 03 (2017) 097. arXiv:1612.04150 https://doi.org/10.1007/JHEP03(2017)097

[29] C. Giunti, General COHERENT constraints on neutrino nonstandard interactions, Phys. Rev. D 101 (3) (2020) 035039. arXiv:1909.00466 https://doi.org/10.1103/PhysRevD.101.035039

[30] P.B. Denton, Y. Farzan, I.M. Shoemaker, Testing large non-standard neutrino interactions with arbitrary mediator mass after COHERENT data, JHEP 07 (2018) 037. arXiv:1804.03660 https://doi.org/10.1007/JHEP07(2018)037

[31] D. Aristizabal Sierra, V. De Romeri, N. Rojas, COHERENT analysis of neutrino generalized interactions, Phys. Rev. D 98 (2018) 075018. arXiv:1806.07424 https://doi.org/10.1103/PhysRevD.98.075018

[32] O.G. Miranda, D.K. Papoulias, G. Sanchez Garcia, O. Sanders, M. Tórtola, J.W.F. Valle, Implications of the first detection of coherent elastic neutrino-nucleus scattering (CEvNS) with liquid argon, JHEP 05 (2020) 130. [Erratum: JHEP 01, 067 (2021)]. arXiv:2003.12050 https://doi.org/10.1007/JHEP05(2020)130

[33] H. Banerjee, B. Dutta, S. Roy, Probing L_μ-L_τ models with CEνNS: a new look at the combined COHERENT CsI and Ar data, Phys. Rev. D 104 (1) (2021) 015015. arXiv:2103.10196 https://doi.org/10.1103/PhysRevD.104.015015

[34] D.K. Papoulias, T.S. Kosmas, R. Sahu, V.K.B. Kota, M. Hota, Constraining nuclear physics parameters with current and future COHERENT data, Phys. Lett. B 800 (2020) 135133. arXiv:1903.03722 https://doi.org/10.1016/j.physletb.2019.135133

[35] D.K. Papoulias, T.S. Kosmas, COHERENT constraints to conventional and exotic neutrino physics, Phys. Rev. D 97 (3) (2018) 033003. arXiv:1711.09773 https://doi.org/10.1103/PhysRevD.97.033003

[36] B. Dutta, D. Kim, S. Liao, J.-C. Park, S. Shin, L.E. Strigari, Dark matter signals from timing spectra at neutrino experiments, Phys. Rev. Lett. 124 (12) (2020) 121802. arXiv:1906.10745 https://doi.org/10.1103/PhysRevLett.124.121802

[37] M. Abdullah, J.B. Dent, B. Dutta, G.L. Kane, S. Liao, L.E. Strigari, Coherent elastic neutrino nucleus scattering as a probe of a Z' through kinetic and mass mixing effects, Phys. Rev. D 98 (1) (2018) 015005. arXiv:1803.01224 https://doi.org/10.1103/PhysRevD.98.015005

[38] S.-F. Ge, I.M. Shoemaker, Constraining photon portal dark matter with texono and coherent data, JHEP 11 (2018) 066. arXiv:1710.10889 https://doi.org/10.1007/JHEP11(2018)066

[39] O.G. Miranda, D.K. Papoulias, O. Sanders, M. Tórtola, J.W.F. Valle, Low-energy probes of sterile neutrino transition magnetic moments, JHEP 12 (2021) 191. arXiv:2109.09545 https://doi.org/10.1007/JHEP12(2021)191

[40] L.J. Flores, N. Nath, E. Peinado, Non-standard neutrino interactions in U(1)' model after COHERENT data, JHEP 06 (2020) 045. arXiv:2002.12342 https://doi.org/10.1007/JHEP06(2020)045

[41] Y. Farzan, M. Lindner, W. Rodejohann, X.-J. Xu, Probing neutrino coupling to a light scalar with coherent neutrino scattering, JHEP 05 (2018) 066. arXiv:1802.05171 https://doi.org/10.1007/JHEP05(2018)066

[42] V. Brdar, W. Rodejohann, X.-J. Xu, Producing a new fermion in coherent elastic neutrino-nucleus scattering: from neutrino mass to dark matter, JHEP 12 (2018) 024. arXiv:1810.03626 https://doi.org/10.1007/JHEP12(2018)024

[43] S. Adamski, et al., COHERENT, Evidence of coherent elastic neutrino-nucleus scattering with COHERENT's germanium array, Phys. Rev. Lett. 134 (23) (2025) 231801. https://doi.org/10.1103/PhysRevLett.134.231801

[44] N. Ackermann, et al., First observation of reactor antineutrinos by coherent scattering, 2025. arXiv:2501.05206

[45] S. Karmakar, et al., TEXONO, New limits on the coherent neutrino-nucleus elastic scattering cross section at the Kuo–Sheng reactor-neutrino laboratory, Phys. Rev. Lett. 134 (12) (2025) 121802. arXiv:2411.18812 https://doi.org/10.1103/PhysRevLett.134.121802

[46] V. Belov, et al., nuGeN, New constraints on coherent elastic neutrino-nucleus scattering by the nuGeN experiment (2025). arXiv:2502.18502 https://doi.org/10.1088/1674-1137/adb9c8

[47] M. Berglund, M.E. Wieser, Isotopic compositions of the elements 2009 (IUPAC technical report), Pure Appl. Chem. 83 (2) (2011) 397–410. https://doi.org/10.1351/PAC-REP-10-06-02

[48] J. Erler, S. Su, The weak neutral current, Prog. Part. Nucl. Phys. 71 (2013) 119–149. arXiv:1303.5522 https://doi.org/10.1016/j.ppnp.2013.03.004

[49] S. Navas, et al., Particle Data Group Collaboration, Review of particle physics, Phys. Rev. D 110 (2024) 030001. https://link.aps.org/doi/10.1103/PhysRevD.110.030001. https://doi.org/10.1103/PhysRevD.110.030001

[50] C. Giunti, K. Kouzakov, Y.-F. Li, A. Studenikin, Neutrino electromagnetic properties, 2024, arXiv:2411.03122 https://doi.org/10.1146/annurev-nucl-102122-023242

[51] J. Bernabeu, L.G. Cabral-Rosetti, J. Papavassiliou, J. Vidal, On the charge radius of the neutrino, Phys. Rev. D 62 (2000) 113012. arXiv:hep-ph/0008114https://doi.org/10.1103/PhysRevD.62.113012

[52] J. Bernabeu, J. Papavassiliou, J. Vidal, On the observability of the neutrino charge radius, Phys. Rev. Lett. 89 (2002) 101802. [Erratum: Phys.Rev.Lett. 89, 229902 (2002)]. arXiv:hep-ph/0206015https://doi.org/10.1103/PhysRevLett.89.101802

[53] R.H. Helm, Inelastic and elastic scattering of 187-Mev electrons from selected even-even nuclei, Phys. Rev. 104 (1956) 1466–1475. https://doi.org/10.1103/PhysRev.104.1466

[54] J. Piekarewicz, A.R. Linero, P. Giuliani, E. Chicken, Power of two: assessing the impact of a second measurement of the weak-charge form factor of ^{208}Pb, Phys. Rev. C 94 (3) (2016) 034316. arXiv:1604.07799 https://doi.org/10.1103/PhysRevC.94.034316

[55] S. Klein, J. Nystrand, Exclusive vector meson production in relativistic heavy ion collisions, Phys. Rev. C 60 (1999) 014903. arXiv:hep-ph/9902259https://doi.org/10.1103/PhysRevC.60.014903

[56] G. Fricke, C. Bernhardt, K. Heilig, L.A. Schaller, L. Schellenberg, E.B. Shera, C.W. de Jager, Nuclear ground state charge radii from electromagnetic interactions, Atom. Data Nucl. Data Tables 60 (1995) 177–285. https://doi.org/10.1006/adnd.1995.1007

[57] G. Fricke, K. Heilig, Nuclear charge radii ^{32}Ge germanium: datasheet from Landolt–Bornstein—Group I elementary particles, nuclei and atoms, Volume 20, 2004. Copyright 2004 Springer-Verlag Berlin Heidelberg, https://materials.springer.com/lb/docs/sm_lbs_978-3-540-45555-4_34. https://doi.org/10.1007/10856314_34

[58] I. Angeli, K.P. Marinova, Table of experimental nuclear ground state charge radii: an update, Atom. Data Nucl. Data Tables 99 (1) (2013) 69–95. https://doi.org/10.1016/j.adt.2011.12.006

[59] J.F. Berger, M. Girod, D. Gogny, Time-dependent quantum collective dynamics applied to nuclear fission, Comput. Phys. Commun. 63 (1991) 365–374. https://doi.org/10.1016/0010-4655(91)90263-K

[60] E. Chabanat, P. Bonche, P. Haensel, J. Meyer, R. Schaeffer, A Skyrme parametrization from subnuclear to neutron star densities. 2. Nuclei far from stablities, Nucl. Phys. A 635 (1998) 231–256. [Erratum: Nucl.Phys.A 643, 441–441 (1998)]. https://doi.org/10.1016/S0375-9474(98)00180-8

[61] M. Hoferichter, J. Menéndez, A. Schwenk, Coherent elastic neutrino-nucleus scattering: EFT analysis and nuclear responses, Phys. Rev. D 102 (7) (2020) 074018. arXiv:2007.08529 https://doi.org/10.1103/PhysRevD.102.074018

[62] R.A. Khaleq, J.L. Newstead, C. Simenel, A.E. Stuchbery, Detailed nuclear structure calculations for coherent elastic neutrino-nucleus scattering, Phys. Rev. D 111 (2025) 033003. https://link.aps.org/doi/10.1103/PhysRevD.111.033003. https://doi.org/10.1103/PhysRevD.111.033003

[63] G. Co', M. Anguiano, A.M. Lallena, Nuclear structure uncertainties in coherent elastic neutrino-nucleus scattering, JCAP 04 (2020) 044. arXiv:2001.04684 https://doi.org/10.1088/1475-7516/2020/04/044

[64] G. Co, M. Anguiano, A.M. Lallena, Tensor force and deformation in even-even nuclei, Phys. Rev. C 104 (1) (2021) 014313. arXiv:2107.09938 https://doi.org/10.1103/PhysRevC.104.014313

[65] M. Atzori Corona, M. Cadeddu, N. Cargioli, F. Dordei, C. Giunti, Reactor antineutrinos CEνNS on germanium: CONUS+ and TEXONO as a new gateway to SM and BSM physics (2025). arXiv:2501.18550

[66] L. Perissé, A. Onillon, X. Mougeot, M. Vivier, T. Lasserre, A. Letourneau, D. Lhuillier, G. Mention, Comprehensive revision of the summation method for the prediction of reactor ν^{-}e fluxes and spectra, Phys. Rev. C 108 (5) (2023) 055501. arXiv:2304.14992 https://doi.org/10.1103/PhysRevC.108.055501

[67] D. Akimov, et al., Measurement of the coherent elastic neutrino-nucleus scattering cross section on CsI by COHERENT, 2021. arXiv:2110.07730

[68] D. Akimov, et al., COHERENT Collaboration data release from the first detection of coherent elastic neutrino-nucleus scattering on argon, 2020, arXiv:2006.12659 https://doi.org/10.5281/zenodo.3903810

[69] J. Colaresi, J.I. Collar, T.W. Hossbach, C.M. Lewis, K.M. Yocum, Measurement of coherent elastic neutrino-nucleus scattering from reactor antineutrinos, Phys. Rev. Lett. 129 (21) (2022) 211802. arXiv:2202.09672 https://doi.org/10.1103/PhysRevLett.129.211802

[70] M. Atzori Corona, M. Cadeddu, N. Cargioli, F. Dordei, C. Giunti, On the impact of the Migdal effect in reactor CEνNS experiments, Phys. Lett. B 852 (2024) 138627. arXiv:2307.12911 https://doi.org/10.1016/j.physletb.2024.138627

[71] Y. Li, G. Herrera, P. Huber, New physics versus quenching factors in coherent neutrino scattering (2025). arXiv:2502.12308

[72] J. Lindhard, V. Nielsen, M. Scharff, P.V. Thomsen, Integral equations governing radiation effects (Notes on atomic collisions, III), Kgl. Danske Videnskab., Selskab. Mat. Fys. Medd. 33, 10 (1963). https://www.osti.gov/biblio/4701226.

[73] A. Bonhomme, et al., Direct measurement of the ionization quenching factor of nuclear recoils in germanium in the keV energy range, Eur. Phys. J. C 82 (9) (2022) 815. arXiv:2202.03754 https://doi.org/10.1140/epjc/s10052-022-10768-1

[74] R. Bouabid, First measurement of CEvNS on germanium by COHERENT, 2024, Presentation at the Magnificent CENNS Workshop, https://indico.global/event/6083/contributions/50001/attachments/24943/42694/m7s_rbouabid_upload.pdf.

[75] M. Atzori Corona, M. Cadeddu, N. Cargioli, F. Dordei, C. Giunti, Refined determination of the weak mixing angle at low energy, Phys. Rev. D 110 (3) (2024) 033005. arXiv:2405.09416 https://doi.org/10.1103/PhysRevD.110.033005

[76] M. Cadeddu, N. Cargioli, J. Erler, M. Gorchtein, J. Piekarewicz, X. Roca-Maza, H. Spiesberger, Simultaneous extraction of the weak radius and the weak mixing angle from parity-violating electron scattering on C_{12}, Phys. Rev. C 110 (3) (2024) 035501. arXiv:2407.09743 https://doi.org/10.1103/PhysRevC.110.035501

[77] M. Deniz, et al., TEXONO, Measurement of Nu(e)-bar -electron scattering cross-section with a CsI(Tl) scintillating crystal array at the Kuo–Sheng nuclear power reactor, Phys. Rev. D 81 (2010) 072001. arXiv:0911.1597 https://doi.org/10.1103/PhysRevD.81.072001

[78] L.B. Auerbach, et al., LSND, Measurement of electron - neutrino - electron elastic scattering, Phys. Rev. D 63 (2001) 112001. arXiv:hep-ex/0101039https://doi.org/10.1103/PhysRevD.63.112001

[79] R.C. Allen, H.H. Chen, P.J. Doe, R. Hausammann, W.P. Lee, X.Q. Lu, H.J. Mahler, M.E. Potter, K.C. Wang, T.J. Bowles, R.L. Burman, R.D. Carlini, D.R.F. Cochran, J.S. Frank, E. Piasetzky, V.D. Sandberg, D.A. Krakauer, R.L. Talaga, Study of electron-neutrino—electron elastic scattering at LAMPF, Phys. Rev. D 47 (1993) 11–28. https://link.aps.org/doi/10.1103/PhysRevD.47.11. https://doi.org/10.1103/PhysRevD.47.11

[80] J. Aalbers, et al., LZ, First dark matter search results from the LUX-ZEPLIN (LZ) experiment, Phys. Rev. Lett. 131 (4) (2023) 041002. arXiv:2207.03764 https://doi.org/10.1103/PhysRevLett.131.041002

[81] D. Zhang, et al., PandaX, Search for light fermionic dark matter absorption on electrons in PandaX-4T, Phys. Rev. Lett. 129 (16) (2022) 161804. arXiv:2206.02339 https://doi.org/10.1103/PhysRevLett.129.161804

[82] E. Aprile, et al., XENON, Search for new physics in electronic recoil data from XENONnT, Phys. Rev. Lett. 129 (16) (2022) 161805. arXiv:2207.11330 https://doi.org/10.1103/PhysRevLett.129.161805

[83] D. Akimov, et al., COHERENT, A D_2O detector for flux normalization of a pion decay-at-rest neutrino source, JINST 16 (08) (2021) P08048. arXiv:2104.09605 https://doi.org/10.1088/1748-0221/16/08/P08048